Journal of
Materials Chemistry C

Materials for optical, magnetic and electronic devices

Accepted Manuscript

This article can be cited before page numbers have been issued, to do this please use: M. Hisada, D. Shimizu and K. Matsuda, *J. Mater. Chem. C*, 2026, DOI: 10.1039/D6TC01255H.

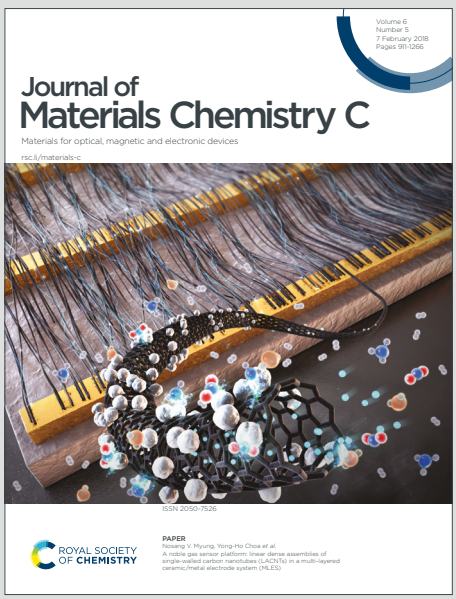

ROYAL SOCIETY OF CHEMISTRY

rsc.li/materials-c

View Article Online
DOI: 10.1039/D6TC01255H

ARTICLE

Heptagon-Fusion as a Molecular Design Strategy for Distorted Acenes

Received 00th January 20xx,
Accepted 00th January 20xx

DOI: 10.1039/x0xx00000x

Masato Hisada,[a] Daiki Shimizu,*[a] and Kenji Matsuda*[a,b]

Distorted acenes have attracted considerable attention owing to their 3-D structures and curvature-dependent properties, which are being used to develop novel organic functional materials. Herein, we report a series of diphenylene-fused acene derivatives incorporating doubly heptagon-fused structures. The introduced heptagons induced two stable conformations, twisted and saddle forms, to the acene cores. Kinetic analyses revealed that the isomerization barrier between the twisted and saddle forms increased with increasing acene length. The twisted isomers exhibited red-shifted absorption spectra compared to the corresponding saddle isomers. Quantum chemical calculations suggest that the narrower band gaps of the twisted isomers primarily originate from the smaller HOMO–LUMO gaps of the twisted acene cores compared with those of the saddle acene cores. These results not only provide a new design strategy for distorted acenes but also provide insights into their unique properties.

Introduction

Introducing distortion into planar π-conjugated systems can yield 3-D structures, such as bowl- and helical-shaped molecules, with curvature-dependent properties.[1–10] The development of distorted π-conjugated systems has provided crucial insights into the design and understanding of novel organic functional materials. In particular, distorted acene derivatives have been extensively explored experimentally by (1) introducing steric hindrance at the periphery,[11–18] (2) tethering with a cross-linking chain (Fig. 1a,b), [19,20] and (3) fusion with helically twisted PAH.[21–23] In the former strategy, firstly proposed by Pascal, the incorporation of bulky peripheral substituents onto acenes induces a crowded and twisted structure with pronounced end-to-end torsion angles (up to 184° for tetrabenzohexacene derivative **1**).[16] However, this strategy is unsuitable for studying chiroptical properties because of the low racemization barrier and fast racemization owing to rotatable substituents. In the second strategy, the incorporation of cross-linking chains onto anthracene cores along the diagonal direction produced twisted anthracenes **2-C*n*** (*n* = 3–6) with end-to-end torsion angles ranging from 23° to 38°, depending on the chain length.[19] However, this method has not yet been applied to larger acenes.

Although the scope of current design strategies for distorted acenes remains limited, twisted acenes exhibit chiroptical properties, red-shifted absorption spectra, and enhanced intersystem crossing rates as end-to-end torsion angles increase.[19,24] Theoretical study suggested that the twist of acenes induces diradical character[25] and reduces the HOMO–LUMO gap (ΔE_{HL}), while bending distortions exert only a minor influence on the ΔE_{HL}.[26]

The introduction of non-hexagonal rings into π-systems leads to non-planar structures.[3,5–7,27–43] Recently, Swager reported a fused decapyrrolyl anthracene **3**, and Uno reported a fused octapyrrolyl naphthalene derivative (Fig. 1c).[31,42] Both compounds contained multiple heptagons and featured twisted acene moieties, with end-to-end torsion angles of 66° for **3** and 26° for the naphthalene derivative. These compounds display low first oxidation potentials ($E^{1/2}_{ox1}$ = −0.40 V for **3** and −0.52 V for the naphthalene derivative), and DFT calculations revealed that the HOMOs are delocalized primarily over the fused pyrrole moieties rather than the acene moieties. While the pyrrole-fusion strategy generates twisted acenes by introducing heptagons, the pronounced substituent effects make it difficult to investigate the relationship between the distortion of acenes and their physical properties.

Recently, we reported heptagon-fused tetracene **Tet7** with a diphenylene-fused structure in two isolable conformations: C_{2h}-symmetric saddle-**Tet7** and D_2-symmetric twisted-**Tet7** (Fig. 1d,e).[43] The twisted isomer possesses a twisted tetracene core, whereas the saddle isomer exhibits a saddle-shaped tetracene core. These two conformers displayed curvature-dependent properties; for instance, the twisted form showed a more red-shifted absorption spectrum and greater photo-oxidation stability than the saddle conformer. While our previous study on **Tet7** highlighted its promising performance in organic FET and solar cells, a systematic investigation of shorter acene cores is essential to fully elucidate how acene length governs core

[a] Department of Synthetic Chemistry and Biological Chemistry
Graduate School of Engineering, Kyoto University
Nishikyo-ku, Kyoto 615-8510, Japan
E-mail: dshimizu@sbchem.kyoto-u.ac.jp, kmatsuda@sbchem.kyoto-u.ac.jp
[b] Fukui Institute for Fundamental Chemistry, Kyoto University
Sakyo-ku, Kyoto 606-8103, Japan
† E-mail: dshimizu@sbchem.kyoto-u.ac.jp, kmatsuda@sbchem.kyoto-u.ac.jp

View Article Online
DOI: 10.1039/D4TC01255N

flexibility, isomerization barriers, and electronic structure. Such fundamental insights provide an indispensable benchmark and design platform for the precise control of next-generation distorted π-electron materials.

Therefore, in this study, we synthesized a series of heptagon-fused naphthalene and anthracene derivatives, **Naph7** and **Ant7**, to generalize the heptagon-fusion strategy as a design approach for introducing in-plane strain into acenes (Fig. 1f). Their physical properties were characterized to examine the impact of acene distortion. It should be noted that a derivative of **Naph7** bearing CF_3 substituents has been reported by Leowanawat *et al.*; its characterization has been limited to absorption and fluorescence properties.[34]

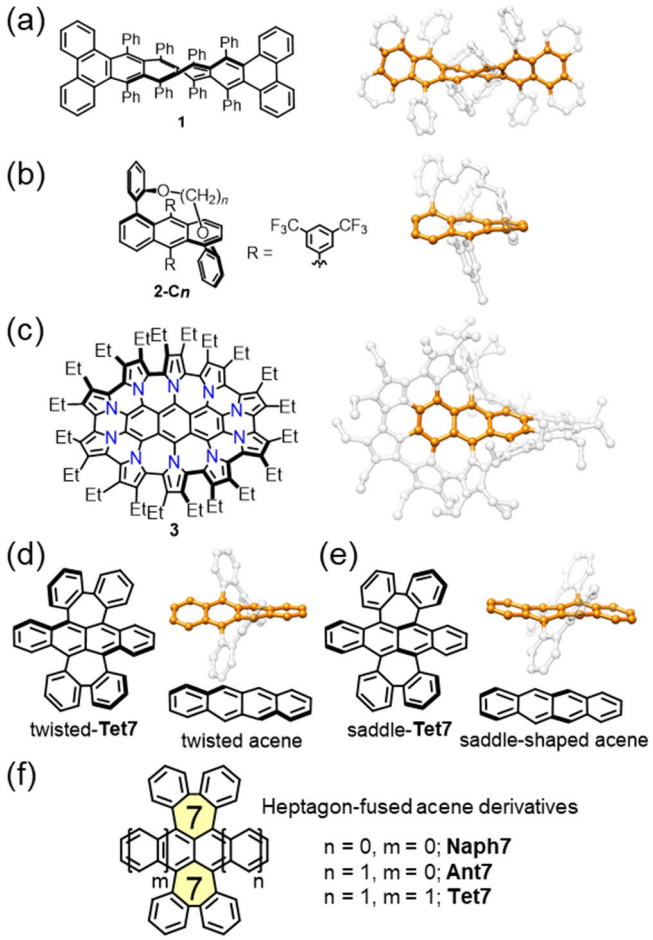

Fig. 1. Structures of (a) highly substituted acene **1**, (b) tethered acenes **2-C*n*** (*n* = 3–6), (c) fused decapyrrolyl acene **3**, (d) twisted-**Tet7**, (e) saddle-**Tet7**, and (f) heptagon-fused acene derivatives. For the X-ray structures, the hydrogen and fluorine atoms were omitted for clarity. Distorted acene moieties are highlighted in orange, while the other moieties are shown in transparent form.[44]

Results and Discussion

Synthesis

The synthesis of heptagon-fused tetracene **Tet7** was previously reported,[43] which employed a reductive coupling reaction as a key step for constructing incorporated heptagons. The widely used oxidative fusion reaction yielded an undesirable fused product when applied to rubrene. Here, we applied the reductive fusion strategy to synthesize heptagon-fused naphthalene **Naph7** and anthracene **Ant7** (Scheme 1). Firstly, compound **4** was prepared from 1,4-diiodobenzene in three steps. The Diels–Alder reaction of **5**/**6** (for **Naph7**/**Ant7**) and *in situ* generated benzyne from **4** afforded the corresponding cycloadducts **7**/**8**. Finally, the intramolecular Yamamoto coupling reaction of **7** and **8** with $Ni(cod)_2$ furnished **Naph7** and **Ant7** in 6% and 21% yields, respectively. An excess amount of $Ni(cod)_2$ was used for the reproducibility of the multi-step fusion process.‡ We consider the primary bottleneck leading to the low yields to be the reductive cyclization step. MS analysis revealed that the major byproducts were partially fused intermediates and dehalogenated species, although their isolation was precluded by the formation of multiple atropisomers with overlapping chromatographic profiles.

The ^{1}H NMR spectrum of **Naph7** displayed five signals in the aromatic region, consistent with its structure (Fig. S11). On the other hand, **Ant7** exhibited two sets of signals in an approximately 1:9 ratio, similarly to **Tet7**, indicating a mixture of two conformers. One minor and two major components were separated by chiral HPLC from the solution of **Ant7**. The separated major components showed mirror-image CD spectra. In addition, both the major and minor conformers of **Ant7** exhibited 11 ^{1}H NMR signals in the aromatic region, indicating a two-fold symmetry. (Fig. S17,S22) These results revealed that the major conformer is chiral twisted-**Ant7** and the minor conformer is achiral saddle-**Ant7**. Interconversion between the two conformers of **Ant7** occurred slowly at room temperature, as discussed later.

Structural analysis

Recently, our group has reported the single crystal structures of twisted-**Tet7** and saddle-**Tet7**.[43] Single crystals of twisted-**Naph7** and twisted-**Ant7** suitable for X-ray crystallographic analysis were obtained by the vapor diffusion method at room temperature (Fig. 2a,b). The twisted structures of both twisted-**Naph7** and twisted-**Ant7** with pseudo-D_2 and pseudo-C_2 symmetry were found in the space groups $I2/a$ and $P2_1/n$, respectively. For twisted-**Naph7**, The asymmetric unit of the crystal contains two independent but almost identical molecules, and one of which is shown in Figure 2 (Table S2). The end-to-end torsion angles (ϕ_1) defined by four carbon atoms at the edge of the acene moiety were 32° for twisted-**Naph7**, 30° for twisted-**Ant7**, and 26° for twisted-**Tet7**, which were comparable with those of the tethered anthracene **2-C*n***.[17] The average torsion angles between the acene moiety and the diphenylene moiety ($\bar{\varphi}$) were 36° (twisted-**Naph7**), 41° (twisted-**Ant7**), and 45° (twisted-**Tet7**).

The structures of the twisted and saddle isomers of the fused acenes were further investigated by DFT calculations. The energy-minimized geometries of all twisted isomers and saddle-**Tet7** closely matched with the corresponding X-ray structures (Table S2, Fig. S30,S31). The calculated saddle-shaped conformers of **Naph7** and **Ant7** are shown in Fig. 2d,e, exhibiting pseudo-C_{2h} (saddle-**Naph7**) and pseudo-C_s (saddle-**Ant7**) symmetry. The calculated end-to-end angles (ϕ_1) of all saddle-conformers were 0°, and the dihedral angles between

the acene core and diphenylene moiety ($\tilde{\varphi}$) were compatible with those of the corresponding twisted conformers (35° for saddle-**Naph7**, 38° for saddle-**Ant7**, and 42° for saddle-**Tet7** (X-ray: 43°)). The acene moiety of the saddle-isomers possesses a doubly bended structure with bend angles (θ_{acd}, θ_{deb}) of (164°, 164°) for saddle-**Naph7**, (166°, 159°) for saddle-**Ant7**, and (161°, 161°) for saddle-**Tet7** (X-ray: 161°, 161°).

View Article Online DOI: 10.1039/D5TC01255H

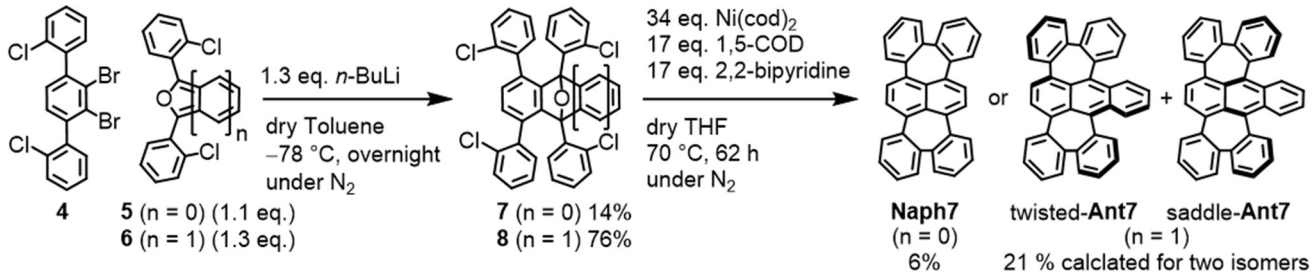

Scheme 1. Synthesis of heptagon-fused naphthalene **Naph7** and heptagon-fused anthracene **Ant7**.

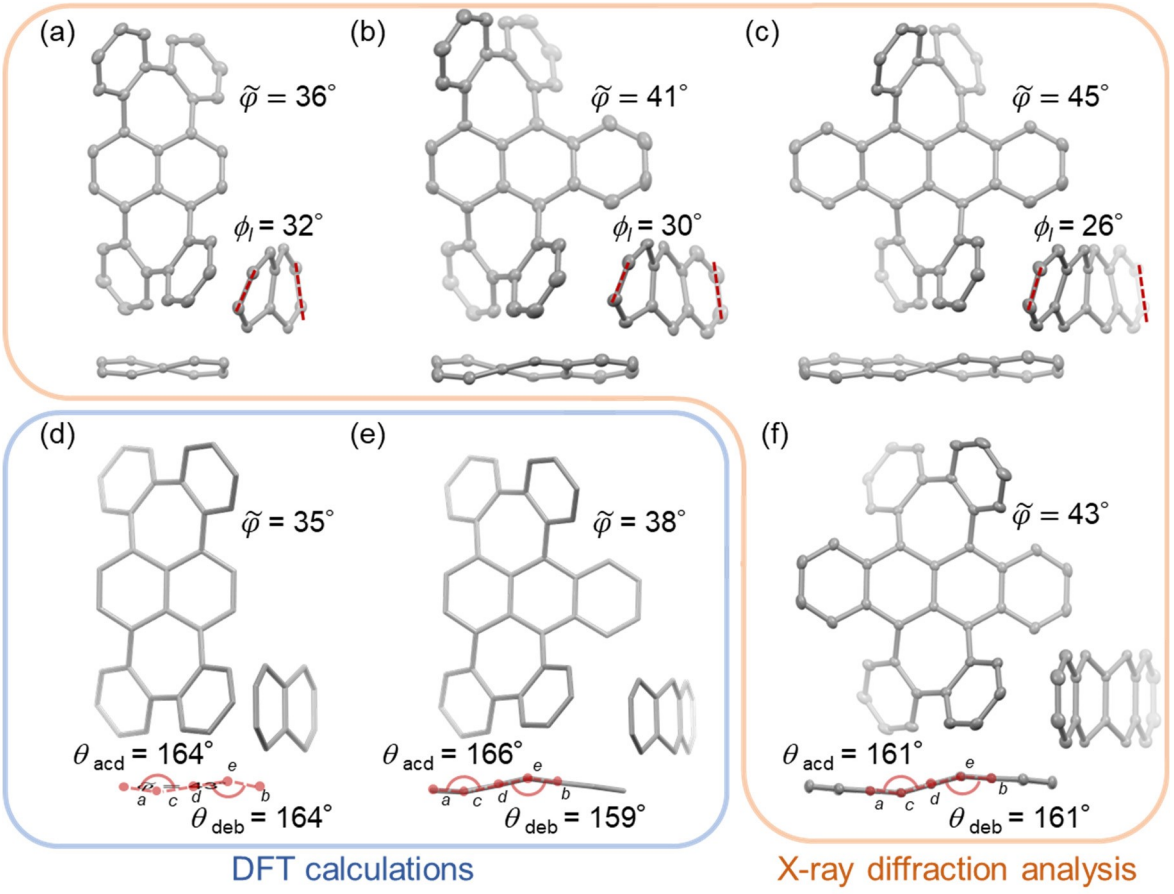

Fig. 2. (a–c, f) X-ray structures of (a) twisted-**Naph7**, (b) twisted-**Ant7**, (c) twisted-**Tet7**,[43] and (f) saddle-**Tet7**[43]; (d,e) optimized structures of (d) saddle-**Naph7** and (e) saddle-**Ant7** calculated at the B3LYP/6-31G(d) level. The average torsion angle φ, end-to-end dihedral angle ϕ_l, and angles θ_{acd} θ_{deb} are shown. Hydrogen atoms are omitted for clarity. In (a,b,c,f), thermal ellipsoids are shown at the 50% probability. One of the two almost identical molecules in the asymmetric unit is shown for twisted-**Naph7** and saddle-**Tet7**.

Kinetics of the isomerization pathway between the conformers

The thermodynamics and kinetics of the isomerization between the saddle and twisted conformers of **Naph7** and **Ant7** were investigated by ^{1}H NMR spectroscopy. While the saddle and twisted conformers of **Ant7** could be separated by HPLC, HPLC analysis on **Naph7** showed a single peak, and the ^{1}H NMR spectra of **Naph7** remained unchanged down to −80 °C in CD_2Cl_2 (Fig. S32). These results indicate the presence of only one conformer in solutions or very rapid interconversion between the conformers of **Naph7**. For **Ant7**, interconversion between the conformers was observed without detectable intermediates or byproducts (Fig. 3a, Fig. S33,S34). Based on the equilibrium ratio of **Ant7** determined by the ^{1}H NMR spectra (saddle/twisted = 0.131/1 at 25 °C, 0.125/1 at 20 °C, 0.123/1 at 15 °C), the isomerization enthalpy (ΔH) and entropy (ΔS) were

View Article Online
DOI: 10.1039/D5TC01255H

estimated to be 4.5 kJ·mol^{-1} and –1.8 J·mol^{-1}·K^{-1}, respectively (Fig. 3b). The rate constants for the saddle-to-twisted ($k_{twist\rightarrow saddle}$) and the twisted-to-saddle ($k_{saddle\rightarrow twist}$) processes were obtained by fitting the data to a reversible first-order interconversion model (See the SI for details). Eyring plots using these rate constants yielded activation enthalpy ($\Delta H^{\ddagger}$) and entropy ($\Delta S^{\ddagger}$) of 63.7 kJ·mol^{-1} and –0.114 kJ·mol^{-1}·K^{-1} for the saddle-to-twisted isomerization, and 68.2 kJ·mol^{-1} and –0.119 kJ·mol^{-1}·K^{-1} for the twisted-to-saddle isomerization, respectively (Fig. S36). Both $\Delta H^{\ddagger}$ were smaller than those of **Tet7** (128.4 kJ·mol^{-1} for twisted-to-saddle isomerization, 143.8 kJ·mol^{-1} for saddle-to-twisted isomerization),[43] which was attributed to reduced repulsion in the transition state.

The observed isomerization dynamics between the conformers were further investigated using quantum chemical calculations at the B3LYP/6-31G(d)//B3LYP/6-311G(2d,p) level (Fig. 3c). In contrast to **Tet7**,[43] the calculations predicted that the twisted isomers of **Naph7** and **Ant7** are the global minima. The saddle conformations were calculated to be 16.3 kJ·mol^{-1} (**Naph7**) and 2.4 kJ·mol^{-1} (**Ant7**) higher than the twisted form at 25 °C. For **Naph7**, the calculated equilibrium ratio (0.999/0.001 = twist/saddle at 25 °C) suggested that **Naph7** predominantly existed as a twisted isomer in solution. The most plausible isomerization pathways are shown in Fig. 3c. The isomerization of **Naph7** proceeds via a transition state, TS1, associated with the inversion of the diphenylene moiety, with an activation barrier of 80.3 kJ·mol^{-1}. In the case of **Ant7**, the isomerization occurs through two transition states, TS1 (89.0 kJ·mol^{-1}) and TS2 (100.0 kJ·mol^{-1}). The structure and energy of TS1 are similar between **Naph7** and **Ant7**. In the case of **Tet7**, isomerization proceeds via TS2 and TS3, and the TS2 of **Ant7** and **Tet7** were also structurally and energetically similar. The highest isomerization barrier of **Tet7** was TS3 at 146.1 kJ·mol^{-1}. These theoretical activation barriers are in good agreement with the experimental results (103.6 kJ·mol^{-1} at 25 °C for **Ant7**, 136.2 kJ·mol^{-1} at 25°C for **Tet7**[43]).

(a)

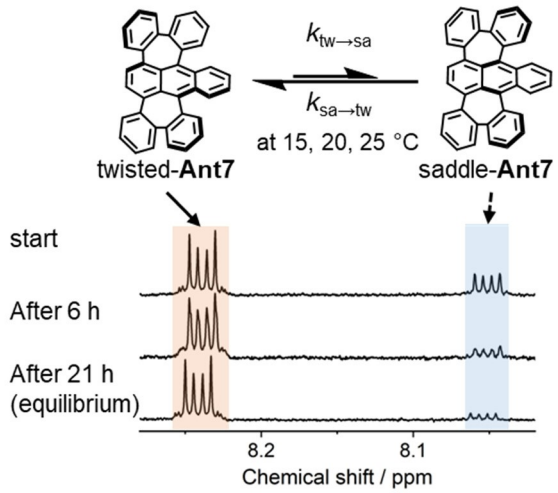

(b)

compound	Naph7	Ant7	Tet7[a]
ΔH_{exp} [b]	N.D.[d]	4.5	−15.4
ΔS_{exp} [c]	N.D.[d]	−0.002	−0.015
ΔG_{exp} at 25 °C[b]	N.D.[d]	5.0	−11.0
ΔG_{calc} at 25 °C[b]	16.3	2.4	−11.6
$\Delta H^{\ddagger}_{tw\rightarrow sa,\ exp}$ [b]	N.D.[d]	68.2	128.4
$\Delta S^{\ddagger}_{tw\rightarrow sa,\ exp}$ [c]	N.D.[d]	−0.119	−0.026
$\Delta G^{\ddagger}_{tw\rightarrow sa,\ exp}$ at 25 °C[b]	N.D.[d]	103.6	136.2
$\Delta G^{\ddagger}_{tw\rightarrow sa,\ calc}$ at 25 °C[b]	80.3	100.0	146.1

[a]ref. 40, [b]kJ·mol^{-1}, [c]kJ·mol^{-1}·K^{-1}, [d]N.D. = Not Determined

(c)

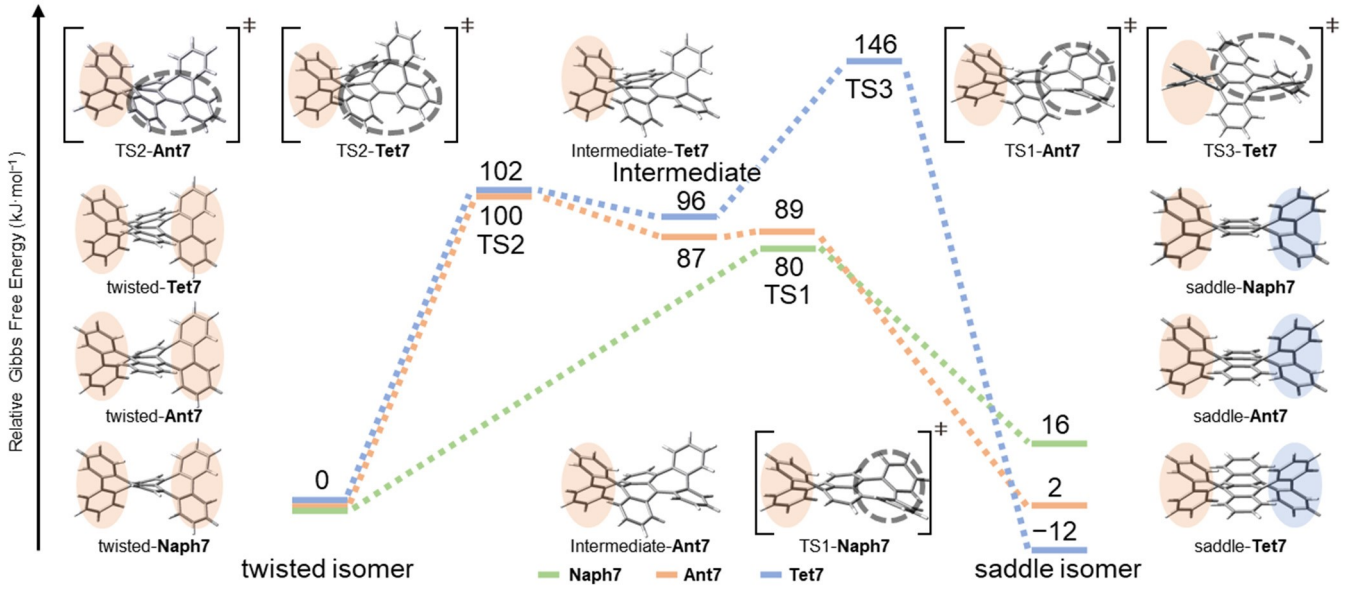

Fig. 3. (a) ^{1}H NMR spectra of twisted-**Ant7** and saddle-**Ant7** during the progress of saddle-to-twisted isomerization in dichloromethane-d_2 at 25°C after 0 h (start), 6 h, and 21 h (equilibrium), (b) thermodynamics parameters of **Naph7**, **Ant7**, and **Tet7**,[43] and (c) isomerization pathways between the twisted and saddle isomers for **Naph7**, **Ant7**, and **Tet7**[43] calculated at the B3LYP/6-31G(d)//B3LYP/6-311G(2d,p) level.

View Article Online DOI: 10.1039/D6TC01255H

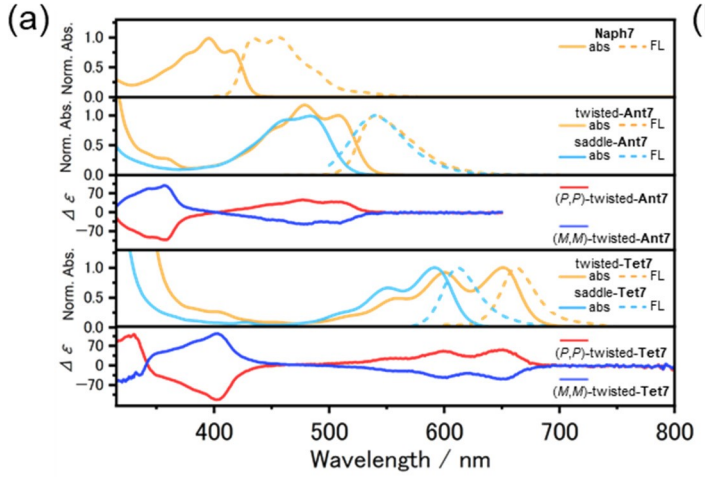

(b)

compound	Naph7	Ant7		Tet7	
isomer	twist[a]	saddle	twist	saddle	twist
λ_{abs} / nm	415	483	508	591	651
ε /10^4 cm^{-1} M^{-1}	1.31	1.50	1.07	1.68	1.13
ΔE_{opt} / eV	2.81	2.34	2.25	1.91	1.77
λ_{em} / nm	435	539	541	611	663
Φ_F	0.20	0.49	0.62	0.23	0.14
$<\tau_s>$ / ns	1.0	4.8	7.7	4.6	5.0
k_f / ns^{-1}	0.200	0.100	0.081	0.050	0.028
k_{nr} / ns^{-1}	0.82	0.11	0.05	0.17	0.17
$\lvert g_{CD}\rvert$ / 10^{-3}	N/A	N/A	3.9	N/A	4.9

[a]predicted by DFT calculation

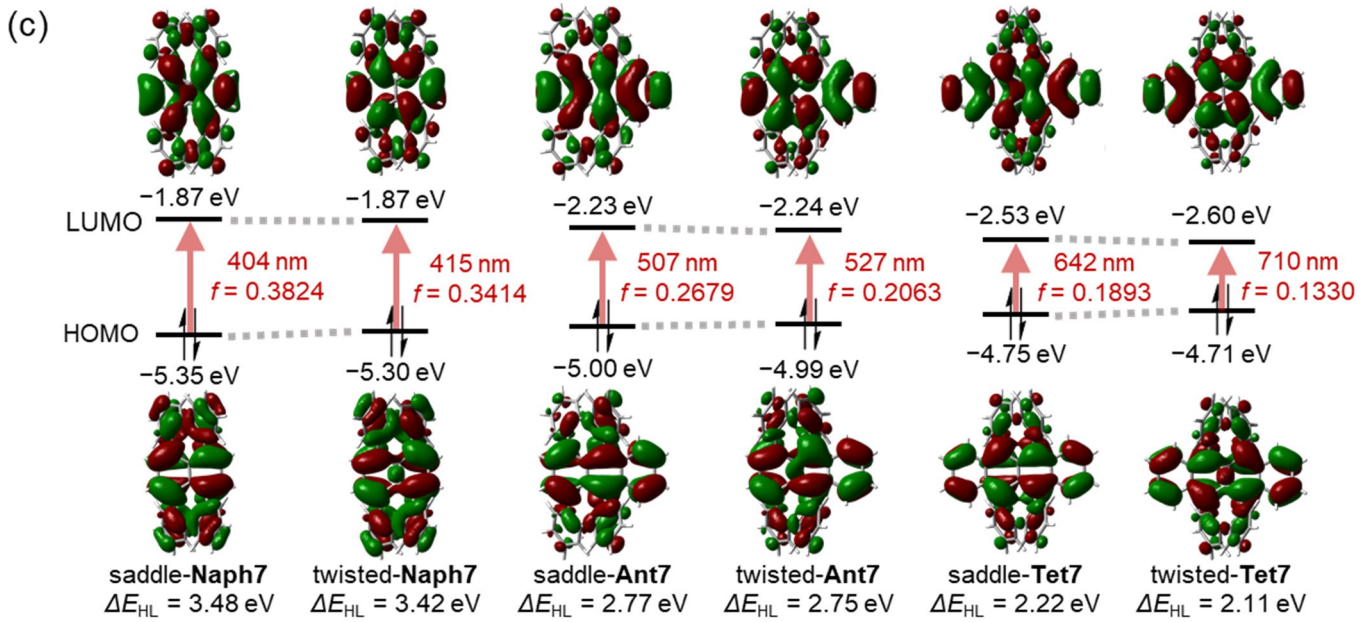

Fig. 4. (a) Absorption, fluorescence, and CD spectra, (b) photophysical parameters of **Naph7**, twisted-**Ant7**, saddle-**Ant7**, twisted-**Tet7**,[43] and twisted-**Tet7**[43] in toluene, and (c) molecular orbital diagram of saddle-**Naph7**, twisted-**Naph7**, saddle-**Ant7**, twisted-**Ant7**, saddle-**Tet7**[43], and twisted-**Tet7**[43] calculated at the (TD-)B3LYP/6-31G(d)//B3LYP/6-311G(2d,p) level.

Photophysical properties

To clarify the impact of molecular conformation on the electronic characteristics, we measured the absorption and fluorescence spectra of **Naph7**, saddle-**Ant7**, and twisted-**Ant7** in toluene (Fig. 4a,b). The spectra of saddle-**Tet7** and twisted-**Tet7** in toluene were reported in our previous work.[43] **Naph7** showed the lowest energy absorption maximum at 415 nm (ε = 1.31 × 10^4 cm^{-1}M^{-1}) and 0-0 emission band at 435 nm (Φ_f = 0.20). For **Ant7** and **Tet7**, twisted isomers exhibited red-shifted absorption spectra relative to the corresponding saddle isomers; 508 nm (ε = 1.07 × 10^4 cm^{-1}M^{-1}) for twisted-**Ant7**, 483 nm (ε = 1.50 × 10^4 cm^{-1}M^{-1}) for saddle-**Ant7**, 651 nm (ε = 1.13 × 10^4 cm^{-1}M^{-1}) for twisted-**Tet7**, and 591 nm (ε = 1.68 × 104 cm^{-1}M^{-1}) for saddle-**Tet7**. The emission spectra of saddle-**Ant7** and twisted-**Ant7** are quite similar (λ_{em} = 539 nm for saddle-**Ant7** and 541 nm for twisted-**Ant7**). The excitation spectra matched their absorption spectra, confirming that the similar emission arises from distinct conformations (Figures S39 and S40). In the case of **Tet7**, the twisted isomer exhibited red-shifted fluorescence spectra compared to the saddle isomer (λ_{em} = 611 nm for saddle-**Tet7**, and λ_{em} = 663 nm for twisted-**Tet7**, Fig. 4a). The saddle and twisted isomers possess compatible dihedral angles between the acene core and the fused diphenylene moiety. Therefore, the observed trend in the optical band gaps is primarily attributed to structural distortion of the acene core, rather than to variations in the π-extension of the diphenylene

View Article Online
DOI: 10.1039/D5TC01251H

units. The fluorescence quantum yield of saddle-**Ant7** (Φ_f = 0.49) is smaller than that of twisted-**Ant7** (Φ_f = 0.62) due to the twice faster non-radiative decay of saddle-**Ant7** (k_{nr} = 0.11 ns^{-1}) compared to that of twisted-**Ant7** (k_{nr} = 0.05 ns^{-1}). The small quantum yield of **Naph7** (Φ_f = 0.20) is also attributed to the high k_{nr} (0.82 ns^{-1}). The fluorescence and excitation spectra of **Naph7** are independent of the excitation and monitoring wavelengths, supporting the conclusion that **Naph7** predominantly exists as a twisted isomer in solution (Fig. S38). The enantiomers of twisted-**Ant7** and twisted-**Tet7** showed mirror-image circular dichroism (CD) spectra ($\Delta\varepsilon$ = 36 $M^{-1}cm^{-1}$, $|g_{CD}|$ = 3.7 × 10^{-3} at 508 nm for **Ant7**, and $\Delta\varepsilon$ = 56 $M^{-1}cm^{-1}$, $|g_{CD}|$ = 4.9 × 10^{-3} at 651 nm for **Tet7**[43]), respectively (Fig. 4a).

The electronic transition characters were disclosed by TD-DFT calculations at the TD-B3LYP/6-311G(2d,p)//B3LYP/6-31G(d) level (Fig. 4c). The observed lowest-energy absorption bands were assigned to the HOMO–LUMO transitions. The calculated frontier orbitals were delocalized over the entire π-electronic system, despite the highly curved structures. The calculated excitation wavelengths of the HOMO–LUMO transitions for twisted isomers (λ = 415 nm for twisted-**Naph7**; λ = 527 nm for twisted-**Ant7**; λ = 705 nm for twisted-**Tet7**[43]) were longer than those of the corresponding saddle isomers (λ = 404 nm for saddle-**Naph7**; λ = 507 nm for saddle-**Ant7**; λ = 642 nm for saddle-**Tet7**[43]), which is consistent with the experimental results. We also calculated the energy-minimized geometry at the S_1 state (Figure S46). The calculation results showed that the difference in emission wavelength between the saddle and twisted isomers increases with increasing acene length (**Naph7** < **Ant7** < **Tet7**).

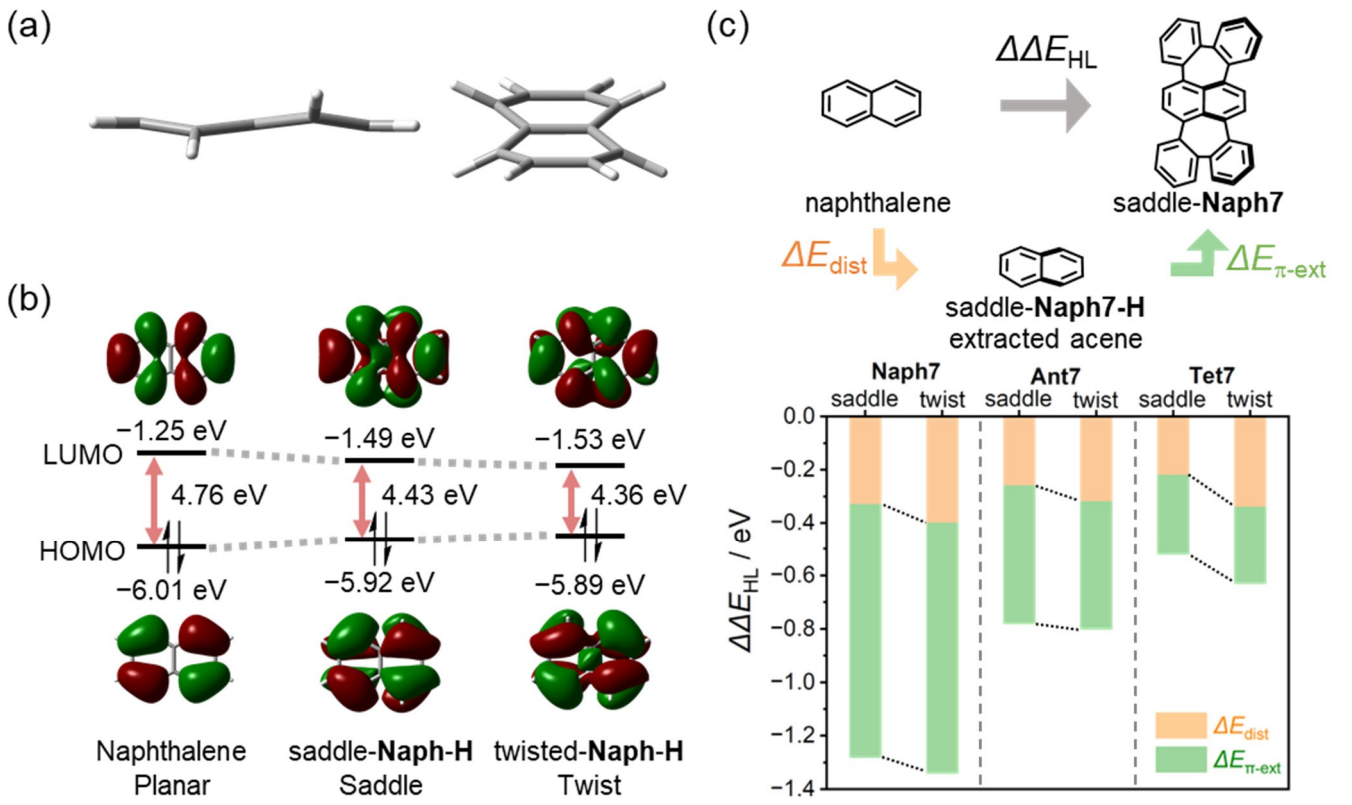

Fig. 5. (a) Structure (top and side views) of saddle-**Naph-H** , (b) molecular orbital diagram of naphthalene, twisted-**Naph7-H**, and saddle-**Naph7-H** calculated at the B3LYP/6-311G(2d,p) level, (c) scheme of deconvolution analysis of $\Delta\Delta E_{HL}$ into distortion and π-extension effects (ΔE_{dist} and $\Delta E_{\pi\text{-ext}}$) for saddle-**Naph7** as an example and summary of the deconvolution.

Distortion effect on the optical band gap of acenes

The optical band gaps of **Naph7**/**Ant7**/**Tet7** are considered as the band gap of the pristine acene being reduced by the structural distortion on the acene core (ΔE_{dist}) and the π-extension of the diphenylene units ($\Delta E_{\pi\text{-ext}}$); *i.e.* ΔE_{HL}(saddle-**Naph7**) = ΔE_{HL}(naphthalene) + ΔE_{dist} + $\Delta E_{\pi\text{-ext}}$ (Fig. 5c). To quantify ΔE_{dist} and $\Delta E_{\pi\text{-ext}}$ for **Naph7**/**Ant7**/**Tet7**, we calculated the corresponding unsubstituted acene cores extracted from their energy-minimized structures (denoted as **Naph7-H**/**Ant7-H**/**Tet7-H**, see Fig. 5a,b and Fig. S44). The difference in optical band gaps between **Naph7-H**/**Ant7-H**/**Tet7-H** and the corresponding pristine acenes was interpreted as the effect of distortion at the acene cores (ΔE_{dist}). Similarly, the difference in optical band gaps between **Naph7-H**/**Ant7-H**/**Tet7-H** and **Naph7**/**Ant7**/**Tet7** was interpreted to be the effect of π-extension ($\Delta E_{\pi\text{-ext}}$). Accordingly, ΔE_{dist} and $\Delta E_{\pi\text{-ext}}$ for **Naph7**/**Ant7**/**Tet7** were calculated and summarized in Fig. 5c and Table 1. The results revealed that both π-extension and structural distortion contribute comparably to ΔE_{HL}. Furthermore, the $|\Delta E_{dist}|$ values of twisted isomers were larger

View Article Online
DOI: 10.1039/D6TC01255H

than those of the corresponding saddle isomers. Conversely, the $|\Delta E_{\pi\text{-ext}}|$ values of twisted isomers were smaller than those of the corresponding saddle isomers. Therefore, the observed narrower optical band gaps of twisted isomers were ascribed to the larger distortion effect on the acene cores. The difference in ΔE_{dist} between the twisted and saddle conformations is consistent with the trend observed in a previous theoretical study, showing that the twisting acenes narrows the ΔE_{HL}, while bending distortions have little effect on ΔE_{HL}.[26]

Table 1. Obtained distortion and π-extension effect on the optical band gaps of **Naph7-H/Ant7-H/Tet7-H**.

Cmpd.	conformation	ΔE_{HL}	$\Delta\Delta E_{HL}$	ΔE_{dist}	$\Delta E_{\pi\text{-ext}}$
Naph7	twisted	3.42	−1.34	−0.40	−0.94
	saddle	3.48	−1.28	−0.33	−0.95
Ant7	twisted	2.75	−0.80	−0.32	−0.48
	saddle	2.78	−0.78	−0.26	−0.52
Tet7	twisted	2.22	−0.63	−0.34	−0.29
	saddle	2.11	−0.52	−0.22	−0.30

Unit: eV. $\Delta\Delta E_{HL} = \Delta E_{dist} + \Delta E_{\pi\text{-ext}}$

Conclusions

In summary, this work demonstrated that the incorporation of heptagons generally induces twisted and saddle-shaped structures into a series of acenes by in-plane strain. Structural and kinetic analyses revealed distinct conformational preferences, where the activation barriers for twisted-to-saddle isomerization increased with acene length (103.6 kJ·mol^{-1} for **Ant7** and 136.2 kJ·mol^{-1} for **Tet7** at 25 °C). Optical measurements and (TD-)DFT calculations showed that twisted isomers exhibited narrower HOMO–LUMO gaps compared to the saddle isomers (e.g., 2.75 eV for twisted-**Ant7** and 2.77 eV for saddle-**Ant7**). Further investigations separately examined the effects of structural distortion and π-extension on the HOMO–LUMO gaps, indicating that the narrower band gaps of the twisted isomer can be ascribed to the induced twist within the acene cores. While the photophysical and chiroptical properties of **Naph7** and **Ant7** (e.g., Φ = 0.20 for **Naph7** and $|g_{CD}| = 3.7 \times 10^{-3}$ for twisted-**Ant7**) are moderate compared to those of larger acenes, the systematic correlation between acene length and isomerization dynamics unveiled here offers crucial guidelines for material optimization. A current limitation of this methodology is the relatively low synthetic yield, which stems from the complex multi-step cyclization process. Future work will focus on optimizing reaction conditions to enhance the scalability and applications of these materials in high-performance organic electronics.

Author contributions

M.H. and D.S. conceived the idea. M.H. performed all experimental studies and wrote the original draft. All authors discussed the results and interpretations. The manuscript was written through the contributions of all authors.

Conflicts of interest

There are no conflicts to declare.

Data availability

The Supporting Information is available free of charge on the RSC Publications website.
Experimental details, spectroscopic data, crystallographic data, electrochemical analysis, and theoretical calculations (PDF)

Acknowledgements

This work was supported by a Grant-in-Aid for Transformative Research Areas (A) "Condensed Conjugation" (JSPS KAKENHI Grant Numbers JP20H05866 and JP20H05868) from MEXT, Japan, and JST FOREST program (Grant Number JPMJFR2427). This work was also supported by a Grant-in-Aid for Scientific Research (B) (JSPS KAKENHI Grant Number 23K26641), a Grant-in-Aid for JSPS Fellows (JSPS KAKENHI Grant Number JP23KJ1377) from JSPS, Japan. The computational resource was provided by the SuperComputer System, Institute for Chemical Research, Kyoto University.

Notes and references

‡. We confirmed that precursors **7** and **8** were completely consumed after the reductive reaction.

1 M. Ball, Y. Zhong, Y. Wu, C. Schenck, F. Ng, M. Steigerwald, S. Xiao and C. Nuckolls, *Acc. Chem. Res.*, 2015, **48**, 267–276.
2 Y. Segawa, H. Ito and K. Itami, *Nat. Rev. Mater.*, 2016, **1**, 15002.
3 M. Saito, H. Shinokubo and H. Sakurai, *Mater. Chem. Front.*, 2018, **2**, 635–661.
4 D. Wu, W. Cheng, X. Ban and J. Xia, *Asian J. Org. Chem.*, 2018, **7**, 2161–2181.
5 S. H. Pun and Q. Miao, *Acc. Chem. Res.*, 2018, **51**, 1630–1642.
6 I. R. Márquez, S. Castro-Fernández, A. Millán and A. G. Campaña, *Chem. Commun.*, 2018, **54**, 6705–6718.
7 M. A. Majewski and M. Stępień, *Angew. Chem. Int. Ed.*, 2019, **58**, 86–116.
8 Y. Liang, M. Tang and Z. Liu, *Chem. Lett.*, 2020, **49**, 1329–1336.
9 Z. Hassan, *Adv. Funct. Mater.*, 2024, **34**, 2311828.
10 R. Kumar, H. Aggarwal and A. Srivastava, *Chem. Eur. J.*, 2020, **26**, 10653–10675.
11 R. A. Pascal Jr, *Chem. Rev.*, 2006, **106**, 4809–4819.
12 M. A. Dobrowolski, M. K. Cyrański and Z. Wróbel, *Phys. Chem. Chem. Phys.*, 2016, **18**, 11813–11820.
13 Y. Yano, H. Ito, Y. Segawa and K. Itami, *Synlett*, 2016, **27**, 2081–2084.
14 T. Fujikawa, Y. Segawa and K. Itami, *J. Am. Chem. Soc.*, 2016, **138**, 3587–3595.
15 W. Fan, T. Winands, N. L. Doltsinis, Y. Li and Z. Wang, *Angew. Chem. Int. Ed.*, 2017, **56**, 15373–15377.
16 R. G. Clevenger, B. Kumar, E. M. Menuey and K. V. Kilway, *Chem. Eur. J.*, 2018, **24**, 3113–3116.
17 W. Matsuoka, K. P. Kawahara, H. Ito, D. Sarlah and K. Itami, *J. Am. Chem. Soc.*, 2023, **145**, 658–666.
18 T. Matsunaga, K. Oki, S. Mori, T. Nishiuchi, M. Higashi, T. Kubo, T. Okujima, H. Uno and M. Takase, *Org. Lett.*, 2025, **27**, 11005–11010.

View Article Online
DOI: 10.1039/D6TC01255H

19 A. Bedi, L. J. W. Shimon and O. Gidron, *J. Am. Chem. Soc.*, 2018, **140**, 8086–8090.
20 I. Shioukhi, A. Agrawal, Y. Deree, B. Bogoslavsky and O. Gidron, *Org. Lett.*, 2025, **27**, 10642–10646.
21 J. A. Weber, E. L. Clennan and N. Arulsamy, European *J. Org. Chem.*, 2022, e202101533.
22 A. Swain, K. Radacki, H. Braunschweig and P. Ravat, *Chem. Sci.*, 2024, **15**, 11737–11747.
23 A. R. Agrawal, I. Shioukhi, Y. Deree, B. Bogoslavsky, O. Shalev, R. Hoffman and O. Gidron, *Angew. Chem. Int. Ed.*, 2025, **64**, e202510423.
24 P. Malakar, V. Borin, A. Bedi, I. Schapiro, O. Gidron and S. Ruhman, *Phys. Chem. Chem. Phys.*, 2022, **24**, 2357–2362.
25 J. E. Norton and K. N. Houk, *J. Am. Chem. Soc.*, 2005, **127**, 4162–4163.
26 A. M. Armon, A. Bedi, V. Borin, I. Schapiro and O. Gidron, *Eur. J. Org. Chem.*, 2021, 5424–5429.
27 W. E. Barth and R. G. Lawton, *J. Am. Chem. Soc.*, 1966, **88**, 380–381.
28 K. Yamamoto, T. Harada, M. Nakazaki, T. Naka, Y. Kai, S. Harada and N. Kasai, *J. Am. Chem. Soc.*, 1983, **105**, 7171–7172.
29 K. Kawasumi, Q. Zhang, Y. Segawa, L. T. Scott and K. Itami, *Nat. Chem.*, 2013, **5**, 739–744.
30 N. Fukui, T. Kim, D. Kim and A. Osuka, *J. Am. Chem. Soc.*, 2017, **139**, 9075–9088.
31 K. Oki, M. Takase, S. Mori, A. Shiotari, Y. Sugimoto, K. Ohara, T. Okujima and H. Uno, *J. Am. Chem. Soc.*, 2018, **140**, 10430–10434.
32 J. M. Farrell, V. Grande, D. Schmidt and F. Würthner, *Angew. Chem. Int. Ed.*, 2019, **58**, 16504–16507.
33 S. H. Pun, Y. Wang, M. Chu, C. K. Chan, Y. Li, Z. Liu and Q. Miao, *J. Am. Chem. Soc.*, 2019, **141**, 9680–9686.
34 K. Kantarod, T. Worakul, D. Soorukram, C. Kuhakarn, V. Reutrakul, P. Surawatanawong, W. Wattanathana and P. Leowanawat, *Org. Chem. Front.*, 2021, **8**, 522–530.
35 M. Hisada, D. Shimizu and K. Matsuda, *Org. Lett.*, 2022, **24**, 3707–3711.
36 M. Hisada, D. Shimizu and K. Matsuda, *J. Org. Chem.*, 2022, **87**, 9034–9043.
37 K. M. Cheung, Y. Xiong, S. H. Pun, X. Zhuo, Q. Gong, X. Zeng, S. Su and Q. Miao, *Chem*, 2023, **9**, 2855–2868.
38 M. Krzeszewski, Ł. Dobrzycki, A. L. Sobolewski, M. K. Cyrański, D. T. Gryko, Saddle-Shaped Aza-Nanographene with Multiple Odd-Membered Rings. *Chem. Sci.* **2023**, *14*, 2353–2360.
39 M. Hisada, D. Shimizu and K. Matsuda, *Chem. Lett.*, 2024, **53**, upae021.
40 S. M. Elbert, O. T. A. Paine, T. Kirschbaum, M. P. Schuldt, L. Weber, F. Rominger and M. Mastalerz, *J. Am. Chem. Soc.*, 2024, **146**, 27324–27334.
41 B. Borrisov, G. M. Beneventi, Y. Fu, Z.-L. Qiu, H. Komber, Q.-S. Deng, P. M. Greißel, A. Cadranel, D. M. Guldi, J. Ma and X. Feng, *J. Am. Chem. Soc.*, 2024, **146**, 27335–27344.
42 A. A. Suleymanov, Q. He, P. Müller and T. M. Swager, *Org. Lett.*, 2024, **26**, 5227–5231.
43 M. Hisada, K. Bulgarevich, Y. Tsutsui, K. Miyata, D. Shimizu, S. Seki, K. Takimiya and K. Matsuda, *J. Am. Chem. Soc.*, 2026, **148**, 6716–6726.
44 E. F. Pettersen, T. D. Goddard, C. C. Huang, G. S. Couch, D. M. Greenblatt, E. C. Meng and T. E. Ferrin, *J. Comput. Chem.*, 2004, **25**, 1605–1612.